Morphological flaring activity predictors: testing and improving

I. Kontogiannis[1], S.-H. Park[2], J. A. Guerra[2] and M. K. Georgoulis[1]

1. Research center for Astronomy and Applied Mathematics, Academy of Athens, Soranou Efesiou Str. 4 Athens, GR-11527, Greece
2. School of Physics, Trinity College Dublin, Dublin 2, Ireland

Abstract

Efficient prediction of solar flares depends on quantities that parameterize the eruptive capability of flare hotspots, solar active regions. Several such quantities have been proposed in the literature, based mostly on magnetograms and/or white light observations. Two of them are the Ising energy and the sum of the total horizontal magnetic gradient. The former has been developed from line-of-sight magnetograms while the latter further utilizes sunspot detections and characteristics, and is derived from continuum images. Aiming to include these parameters in an automated prediction scheme, we test their applicability on regular photospheric magnetic field observations provided by the Helioseismic Magnetic Imager (HMI) instrument onboard the Solar Dynamics Observatory (SDO). We test their efficiency as predictors of flaring activity on a representative sample of active regions and investigate possible modifications. We find that both quantities are efficient flare predictors, achieving more significant probabilities than the unsigned magnetic flux, while their efficiency may improve with appropriate modifications. This study has received partial support by the EU Horizon 2020 FLARECAST Project (Grant Agreement No. 640216)

Extraction of morphological parameters

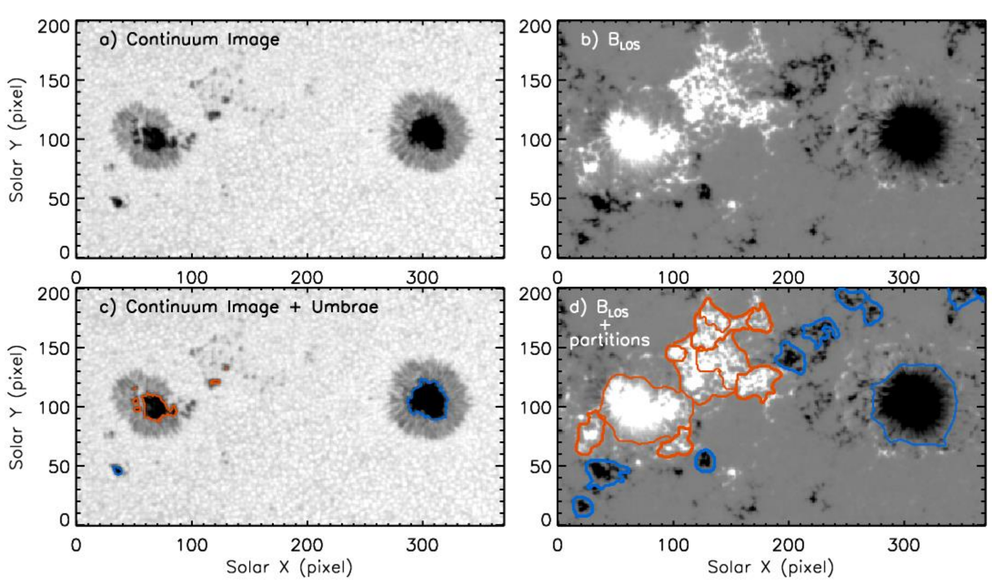

Fig.1 *a – b) Continuum image and co-temporal line-of-sight magnetogram of NOAA AR 11611. c) continuum image with overlaid contours of the positive (red) and negative (blue) umbral areas produced with the method of Padinhatteeri et al. (2016). d) line-of-sight magnetogram with overlaid contours of the magnetic partitions produced with the method of Barnes et al. (2005).*

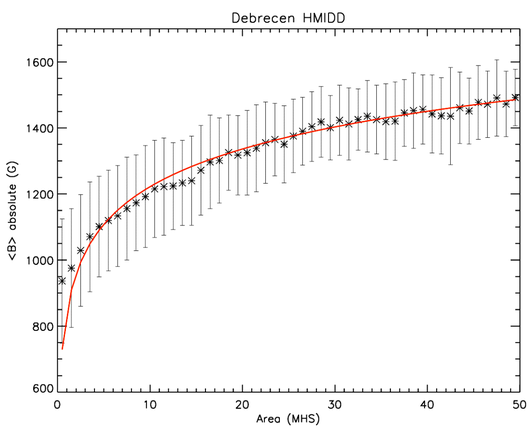

Fig.2. *Absolute mean magnetic field as a function of umbral area (black stars) and the overplotted fitted curve (red line). The values are taken from the database of the Debrecen Observatory and are calculated for the HMI data between 2010 and 2014. Only active regions within 10º from the central meridian are taken into account.*

Sum of the Horizontal Magnetic Gradient, G_S

- Introduced by *Korsós et al. (2014, 2015)* and *Korsós & Erdélyi (2016)*.
- Heliophysical Observatory, Debrecen database: sunspot numbers, umbral/penumbral areas, positions, etc (http://fenyi.solarobs.csfk.mta.hu/en/databases/SOHO/ *Baranyi et al. 2016*).

$$G_S = \left| \sum_{i,j} \frac{B_{p,i}A_{p,i} - B_{n,j}A_{n,j}}{d_{i,j}} \right|$$

Bp (*Bn*) the mean magnetic field of the positive (negative) umbrae and *Ap* (*An*) the corresponding area.

- Continuum images: extraction of umbral and penumbral areas (*Györy 1998*).
- LOS magnetograms: to correspond each umbral area *A* to a mean magnetic field <*B*>.
- <*B*> = *f(A)* is fitted to produce the calibration relation: <*B*> = *f(A)* = $K_1 \cdot ln(A) + K_2$ (***Fig. 2***). For HMI data : K_1 = *165 G/MSH and* K_2 = *842.16 G*. These values are used to convert umbral areas to mean magnetic field.
- Umbral areas are determined following *Padinhatteeri et al. (2016)*, which is based on threshold values of intensity and magnetic flux density for umbrae and penumbrae area (see ***Fig.1a, b*** and ***c***).

Ising Energy calculations

- Introduced by *Ahmed et al. 2010* to describe the interaction of opposite polarity elements of an active region.
- A line-of-sight magnetogram is used.
- Low absolute value pixels (less than 100 G) are eliminated (set to 0). E_{Ising} is calculated via $E = -\sum_{ij}^{N} \frac{S_i S_j}{d^2}$

S = +1 (-1) for a positive (negative) pixel and *d* the distance between pairs of opposite polarity pixels (***Fig.3a***).

We introduce:

- $E_{Ising,part}$, calculated for the pairs of opposite polarity partitions (***Fig.3b***), produced using a partitioning scheme (*Barnes et al. 2005*). Thresholds on minimum magnetic flux density (*100* G), minimum area (*40* pixel) and minimum enclosed magnetic flux ($5 \cdot 10^{19}$ Mx).
- $E_{Ising,spot}$, i.e. the Ising energy for the opposite polarity umbrae detected for the calculation of G_S (***Fig.3c***).

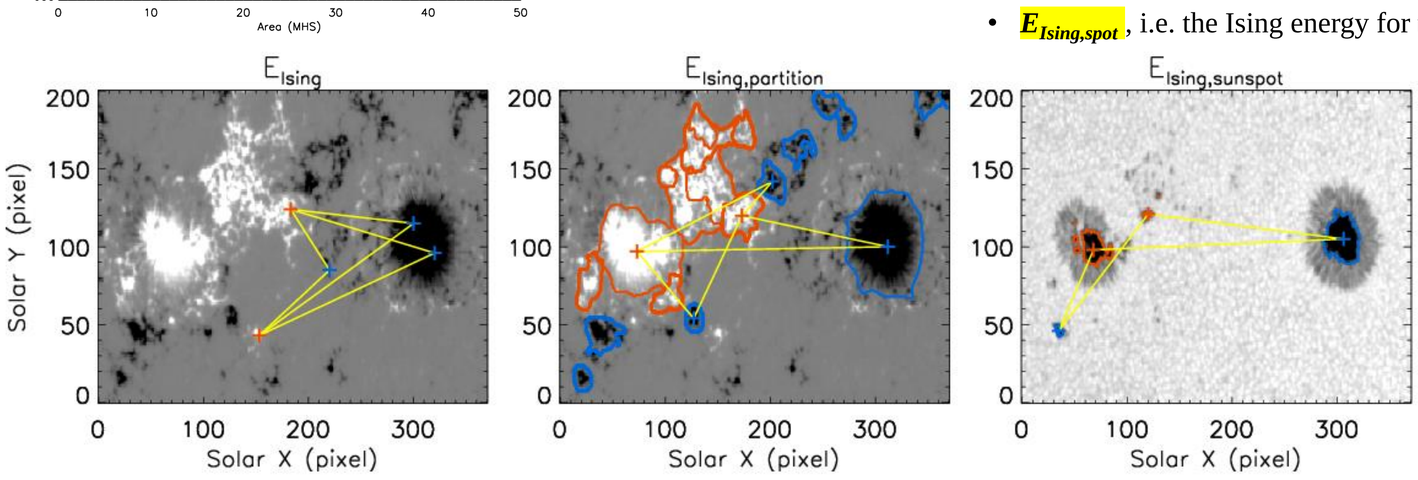

Fig.3. *Examples demonstrating the definition of the interacting opposite polarity elements for the three types of Ising Energy. a) pairs of opposite polarity pixels for E_{Ising}, b) pairs of opposite polarity partitions for $E_{Ising,part}$ and c) pairs of opposite polarity umbrae for $E_{Ising,spot}$. In all panels, red (blue) stands for positive (negative) magnetic flux and yellow lines mark the distances between opposite polarity pairs.*

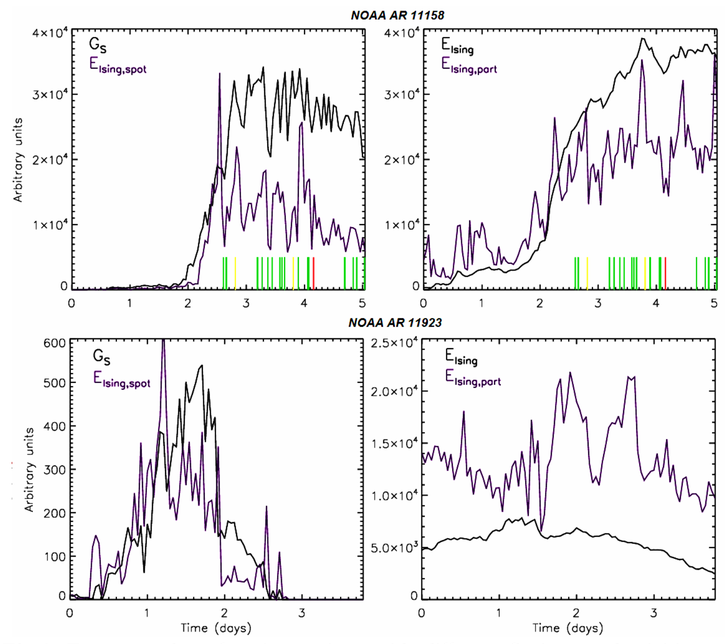

Fig.4. *Two examples of active regions with different flaring productivities and the corresponding time-series of the four parameters. Upper row: The flare productive NOAA AR 11158 observed between 10/02/2011 and 15/02/2011, which produced one X-class flare (red vertical line) and several M- and C-class flares (green and yellow lines correspondingly). Lower row: The quiet NOAA AR 11923, observed between 12/12/2013 and 15/12/2013 and produced no flares.*

Results

Four parameters are tested for their predictive potential:

- ***The Sum of the Horizontal Magnetic Gradient,*** G_S
- ***The Ising energy of the original magnetogram,*** E_{Ising}
- ***The Ising energy of the partitioned magnetogram,*** $E_{Ising,part}$
- ***The Ising energy of the sunspot distribution,*** $E_{Ising,spot}$

- Initial testing (***Fig.4***) on time series of HMI Active Region Patches (SHARP) data (*Bobra et al. 2014*).
- Representative sample of 9454 SHARP data: 336 randomly selected days between September 2012 and May 2016, 6 h cadence.
- The associated flaring activity within 24 h was inferred from the Geostationary Operational Environmental Satellite (GOES) flare catalogue (http://www.swpc.noaa.gov).
- Bayesian inference of the predictive capability of the four parameters, against that of the total unsigned magnetic flux:

$$p = \frac{F+1}{N+2} \qquad \delta p = \sqrt{\frac{p(1-p)}{N+3}}$$

N and *F* are the numbers of all and flaring AR respectively, with a property value higher than a threshold ***(Fig.7)***.

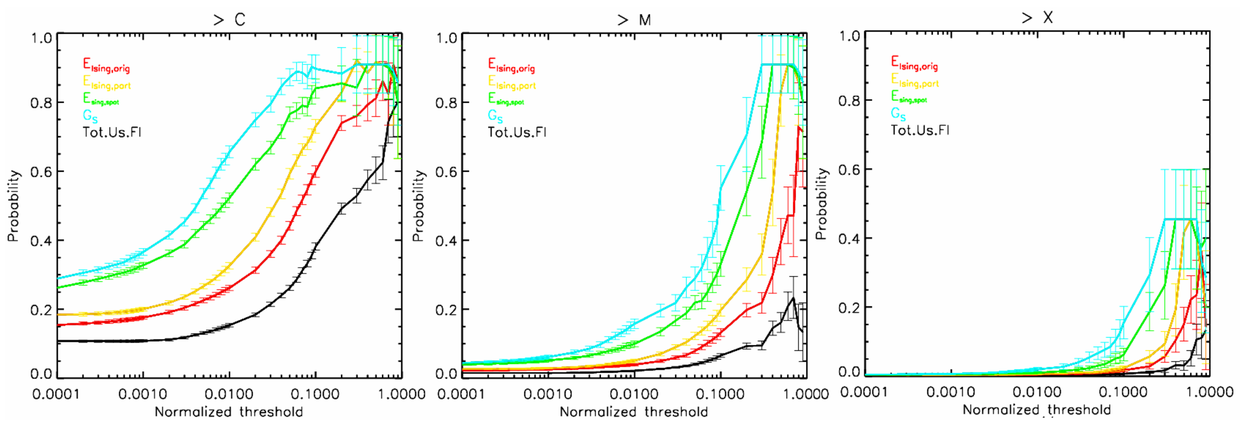

Fig.5. *Bayesian inferred probabilities for flares stronger than C1.0 (left), M1.0 (middle) and X1.0 (right) for various thresholds of the four parameters and the total unsigned magnetic flux. To facilitate comparison, the thresholds are normalized to the maximum value of each parameter.*

Conclusions

- AR with high flare productivity statistically exhibit higher values of G_S, E_{Ising}, $E_{Ising,part}$ $E_{Ising,spot}$. For G_S and $E_{Ising,spot}$, this difference is more than one order of magnitude (***Fig. 4***).
- These parameters also show potential in distinguishing between flare-quiet and flare-productive phases of AR evolution (***Fig. 4, upper row***).
- All four parameters show a better predictive potential than the total unsigned magnetic flux (***Fig. 5***). Hence, they are worth considering in automated prediction schemes.
- The sum of the horizontal gradient seems to be a somewhat better forecaster for this sample (***Fig. 5***).
- Ising energy becomes significantly more effective as a flare predictor when magnetic partitions or the umbral areas are considered as the interacting elements ($E_{Ising,part}$, $E_{Ising,spot}$) (***Fig.5***).

Acknowledgments

This research has been financed by the European Union's Horizon2020 research and innovation programme under grant agreement No.640216 for the "Flare Likelihood And Region Eruption foreCASTing" (Flarecast) project. The data used here are courtesy of NASA/*SDO* and the HMI science team, as well as the Geostationary Satellite System (*GOES*) team.

References

Ahmed, O., Qahwaji, R., Colak, T., et al. 2010, *Vis. Comput.* **26**, 385.
Baranyi, T., Györi, L., & Ludmány, A., 2016, Sol. Phys., 291, 3081
Barnes, G., Longcope, D. W., & Leka, K. D. 2005, ApJ, 629, 561
Bobra, M. G., Sun, X., Hoeksema, J. T., et al. 2014, Sol. Phys., 289, 3549
Györy, L., 1998, Sol.Phys., 180, 109
Korsós, M.B., Baranyi, T., & Ludmány, A., 2014, ApJ, 789, 107
Korsós M.B., Ludmány, A., Erdélyi, R., & Baranyi, T., 2015, ApJ, 802, L21
Korsós, M.B., & Erdélyi, R., 2016, ApJ, 823, 153
Padinhatteeri, S., Higgins, P.A., Bloomfield, S.D., & Gallagher, P.T., 2016, Sol. Phys, 291, 41